Journal of the Meteorological Society of Japan

EARLY ONLINE RELEASE

The DOI for this manuscript is
DOI:10.2151/jmsj.2022-026
J-STAGE Advance published date: February 18th, 2022
The final manuscript after publication will replace the preliminary version at the above DOI once it is available.

Extreme precipitation in 150-year continuous simulations by 20-km and 60-km atmospheric general circulation models with dynamical downscaling over Japan by a 20-km regional climate model

Ryo Mizuta, Masaya Nosaka, Toshiyuki Nakaegawa, Hirokazu Endo, Shoji Kusunoki, Akihiko Murata, and Izuru Takayabu

Meteorological Research Institute, Tsukuba, Ibaraki 305-0052, Japan

Corresponding author: Ryo Mizuta, Meteorological Research Institute, Tsukuba, Ibaraki 305-0052, Japan. E-Mail: rmizuta@mri-jma.go.jp.

Abstract

Continuous simulations from the middle of the 20th century to the end of the 21st century were performed using a 20-km atmospheric general circulation model (AGCM), and a 60-km AGCM with dynamical downscaling via a 20-km regional climate model (RCM), to explore the transitional changes in regional extreme events. The representative scenario simulations by the AGCMs followed the protocol of the High Resolution Model Intercomparison Project experiments. In addition, ensemble simulations using four emission scenarios were conducted using the 60-km AGCM with 20-km RCM downscaling.

Regardless of the emission scenario used, the global-mean relative increase in annual maximum daily precipitation (Rx1d) was roughly proportional to the increase in the global-mean surface air temperature (SAT), consistent with previous results from coarser-resolution climate models. It means that the relationship is also valid for a higher-resolution model. A similar correlation between Rx1d and SAT was seen also in the values averaged over the Japanese land area in the 20-km AGCM and the 20-km RCM simulations after applying a 10-year running mean. However, it was not so clear in the 60-km AGCM, mainly due to insufficient grid points over land in Japan in the 60-km AGCM due to too large noise. It suggests that transitional changes in Rx1d at regional scales such as the Japanese land area can only be represented by using a model resolution as high as 20 km, unless using ensemble simulations.

1. Introduction

Changes in extreme events, caused by global warming, are having a significant effect on the magnitude and frequency of natural disasters, as well as on agricultural activity and water resource management, and there is a need for more detailed forecasts of such changes at the regional scale. To study extreme phenomena such as heavy rainfall, long-term simulations that cover several decades or more are required at a resolution that is high enough to accurately represent heavy rainfall. Therefore, we have used our atmospheric general circulation model (AGCM) with horizontal resolutions of 60 and 20 km, together with dynamical downscaling via our regional climate model (RCM) at horizontal resolutions of 20, 5, 2, and 1 km. Previous studies have carried out time-slice simulations of future specific years (e.g., 2075–2099; Kitoh et al. 2016), and future years at specific warming levels (e.g., 4°C, 2°C, and 1.5°C warming; Mizuta et al. 2017; Fujita et al. 2019; Nosaka et al. 2020; Ishii and Mori 2020), with prescribed sea surface temperature (SST) warming derived from the models used in the Coupled Model Intercomparison Project (CMIP).

It has been shown that some recent heavy rainfall events, as well as extreme temperature events were influenced by global warming (Imada et al. 2020). There is an increasing need for better information regarding the temporal evolution of these extreme events from now to the end of this century, and on the timing of the emergence of the signal associated with any changes above the noise of natural variability (Hawkins et al. 2020). Large changes that fall outside the range of past experience could have a significant impact on natural disasters, water resources, agriculture, ecosystems, and human health. We also need information on how such changes depend on the emissions scenarios. This information is becoming increasingly important, especially for the development of adaptation policies for global warming.

Therefore, in this study, we performed high-resolution continuous simulations from 1950 to 2099 using the same model as our previous time-slice simulations. Continuous simulations with a 60-km resolution AGCM have already been shown to be useful for the analysis of the temporal evolution of changes in extreme rainfall events such as tropical cyclones (Sugi and Yoshimura 2012) and precipitation intensity over East Asia (Kusunoki and Mizuta 2013). Here, we used a 20-km AGCM and 20-km RCM, as well as a 60-km AGCM to facilitate comparisons among different resolutions. The representative scenario simulations with the AGCMs are conducted as the High Resolution Model Intercomparison Project (HighResMIP; Haarsma et al. 2016) experiments. HighResMIP is one of the CMIP6 (Eyring et al. 2016) experiments to compare the impact of increasing the horizontal resolution of climate models on climate reproduction among climate models from various organizations around the world. In addition, ensemble simulations based on four emissions scenarios were conducted using the 60-km AGCM with 20-km RCM downscaling.

Here, we will document the detailed experimental design and temporal changes in the surface temperature and precipitation, then show the relationships between the warming and the extreme precipitation increase in the global and Japanese regions, and their differences among the experiments.

2. Models and experimental design

We used the MRI-AGCM3.2 model (Mizuta et al. 2012) with horizontal resolutions of 20 and 60 km for the global simulations (hereafter AGCM20 and AGCM60, respectively), and the NHRCM model (Sasaki et al. 2008; Murata et al. 2015) with a horizontal resolution of 20 km for the dynamical downscaling around Japan (hereafter RCM20). AGCM60 and RCM20 were the same models and settings as those used in the Database for Policy Decision-Making for Future Climate Change (d4PDF; Mizuta et al. 2017), except that the RCM20 has been modified to produce sea ice depending on the SST, since the sea ice over Okhotsk Sea is not represented in the RCM20 of d4PDF. AGCM20 has the same parameter settings as AGCM60 except for the integration time step (10 minutes for AGCM20 and 20 minutes for AGCM60), which are also the same ones as the model used in previous studies (e.g., Murakami et al. 2012; Kitoh and Endo 2016).

The future scenarios used in this study were the CMIP5 RCP8.5 scenario for AGCM20 and the RCP8.5, RCP6.0, RCP4.5, and RCP2.6 scenarios for AGCM60 with the RCM20 downscaling. The RCP8.5 is the highest emission scenario, where greenhouse gas emissions continue to grow unmitigated, and the RCP2.6 is a mitigation scenario aiming to limit the increase of global mean temperature to 2°C. Each simulation was conducted between 1950 and 2099. Simulations of the historical climate up to the present time (1950–2014) were performed based on the observational boundary conditions with different initial values and connected to the respective scenario experiments (2015–2099). The multiple historical simulations are used to evaluate the internal variability of the atmosphere as the ensemble spread.

For the boundary conditions settings, we followed the HighResMIP (Haarsma et al. 2016) protocol. The settings are listed in the right column of Table S1. For the historical simulation, we used the 0.25° daily gridded SST and sea ice concentrations from HadISST2.2 dataset (Kennedy et al. 2017), the same SST as in the *highresSST-present* experiment of the HighResMIP. As specified in the HighResMIP, the same settings as in the CMIP6 *historical* experiments (O'Neill et al. 2016) are used for ozone, volcanic aerosols, greenhouse gases, and solar activity. For non-volcanic aerosols, we used the monthly mean three-dimensional output from the *historical* experiments by MRI-ESM2 (Yukimoto et al. 2019), instead of implementing the recommended HighResMIP protocol into MRI-AGCM.

For the future climate simulations, the CMIP5 model-averaged temperature increase is added to the observed SST and sea ice concentrations (see below). For ozone, volcanic aerosols, greenhouse gases, and solar activity, the protocols of the CMIP6 *ssp585*, *ssp460*, *ssp245*, and *ssp126* experiments are used, and the monthly mean outputs from the *ssp585*, *ssp460*, *ssp245*, and *ssp126* experiments by MRI-ESM2 are used for the non-volcanic aerosols.

For the RCP8.5 scenario experiments, we used the same SST as in the *highresSST-future* experiment of the HighResMIP, in which the SST increase averaged over eight CMIP5 models (ACCESS1-0, ACCESS1-3, GFDL-CM3, IPSL-CM5A-LR, IPSL-CM5A-MR, MPI-ESM-MR, CNRM-CM5, and HadGEM2-ES), that were selected based on their representation of Arctic sea ice variability, are used. As this is a continuous simulation, consideration was given to avoid major discontinuities around 2015. The SST for 2015 was based on the observed HadISST data. After 2016, monthly deviations from the 2005–2025 average were calculated for each model. Nine-year running means of the monthly deviations were averaged across all models and added to the 2007–2015 average of HadISST. This defines the SST without interannual variability after 2016 (thick black dashed line behind red lines in Fig. 1a). Next, as a component of interannual variability, daily deviations from the 9-year running mean of HadISST were calculated for 1980–2015, and the time series were added to it repeatedly over the periods 2016–2051, 2052–2087, and 2088–2099 (red lines in Fig. 1a). Note that, for smoother transitions, the values on January of 2016, 2052, and 2088 are linearly interpolated with those at the end of the previous year. For the sea ice concentration, equations expressing sea ice concentration as a function of SST are constructed for HadISST and CMIP5 models, respectively. The sea ice concentration in the future simulations is estimated by inputting the generated future SST into it. Linear interpolation of the two for 2016–2030 is used, and the latter equation is used for 2031–2099. More details can be found in the document referenced in https://github.com/PRIMAVERA-H2020/HighResMIP-futureSSTSeaice.

For the other RCP scenarios, we used the same setup as for the *highresSST-future* experiment, but with the SST changes from the RCP6.0, RCP4.5, and RCP2.6 scenarios. However, because not all of the eight models used for the RCP8.5 SST provide the other scenario experiment results, the same 28 CMIP5 models (21 models for RCP6.0) as Mizuta et al. (2014) are used for the other scenario SST future changes. Figure 1(a) shows the time series of the SSTs for the four RCP scenarios. As RCP6.0 is radiatively forced below RCP4.5 until around 2070, the SSTs are also below those of RCP4.5. Figure S1 shows the SST warming patterns from the end of the 20th century to the end of the 21th century. Although the large-scale distributions for the RCP8.5 scenario (Fig. S1a) are similar to those from the previous 20-km AGCM time-slice simulations (Kitoh and Endo 2016), the detailed patterns differ because of the different methods and number of CMIP5 models used.

The differences in the boundary conditions compared with our previous time-slice simulations and d4PDF are shown in Table S1. We confirmed that, even with these differences, the simulations covering the historical period generated a similar climate representation performance. Figure S2 shows the climatological seasonal precipitation from 1979 to 2003, and demonstrates that the AGCM20 and AGCM60 results from this study (Fig. S2c, d, g, h) have a similar precipitation distribution to the previous 20-km AGCM time-slice (Fig. S2a, b) and d4PDF (Fig. S2e, f) results.

To evaluate the model representation around Japan, we used observational data of Japan Meteorological Agency. We used data at all stations in Japan that have long-term observation from 1950 to 2020 (134 stations) to calculate the annual maximum daily precipitation (Rx1d), and selected non-urban 15 stations (Abashiri, Nemuro, Suttsu, Yamagata, Ishinomaki, Fushiki, Iida, Choshi, Sakai, Hamada, Hikone, Tadotsu, Miyazaki, Naze, and Ishigakijima), the same as those in Japan Meteorological Agency (2021), for the surface air temperature (SAT) to avoid including the effects of urbanization.

3. Changes in surface air temperature and precipitation

The time series of global-mean SAT in the simulations are shown in Fig. 1b. The SAT increases almost in proportion to the increase in the given SST (Fig. 1a). The warming above the level of 1950–1979 at 2070–2099 is 1.3°C, 2.0°C, 2.4°C, and 3.9°C for the RCP2.6, RCP4.5, RCP6.0, and RCP8.5 scenario, respectively. These temperature increases are close to the changes in the multi-model averages of the CMIP5 experiments (Collins et al. 2013). Figure 1c shows the time series of the 10-year running mean of SAT averaged over the Japanese land grids from both the global and regional models, compared with the average of the observed data. Although the same SST was prescribed for all simulations until 2014 (Fig. 1a), these narrow regional averages show a spread among the members even in the 10-year running mean. Therefore, we can assume that the SAT in the future simulations also contains such uncertainty. This spread is about 0.5°C both in the AGCM60 simulations and in the RCM20 simulations. The average SAT for the period 2011–2020 in the observations is 0.97°C higher than the average for 1950–1979. The warming over Japan at 2070–2099 in RCM20 is 1.3°C, 2.6°C, 3.1°C, and 5.1°C for the RCP2.6, RCP4.5, RCP6.0, and RCP8.5 scenario, respectively. It is about 30% larger than the global-mean warming, except for the RCP2.6 scenario.

Figure 2 compares the changes in seasonal mean precipitation and Rx1d for the RCP8.5 simulations of AGCM20, and for the RCP8.5 and RCP2.6 simulations of AGCM60. In the same RCP8.5 simulations, there are no noticeable differences between AGCM20 and AGCM60 in terms of mean precipitation and annual maximum daily precipitation (Fig. 2a–f). The general patterns of change in the AGCMs are consistent with the results from our previous AGCM time-slice simulations (Kitoh and Endo 2016) and d4PDF (Mizuta et al. 2017), although there is a difference near the tropics due to the slight difference in the patterns of SST change (Fig. S3). Comparing the RCP8.5 and RCP2.6 simulations of AGCM60 (Fig. 2d–i), while the change is proportional to the amount of temperature increase over a large part of the world, there are some places where signs of this change differ depending on the scenario, especially in the summer western Pacific region including Japan (Fig. 2e, h). Such differences are more significant for changes in annual maximum daily precipitation (Fig. 2f, i).

Those changes in the RCP8.5 for the area around Japan are shown in Fig. 3, which compares the results from RCM20 in addition to those from the AGCM simulations. The differences between the resolutions and the models are small in winter (Fig. 3a, d, g), with a decrease over the southern coast of Japan and an increase over northern Japan. These changes correspond to the northward shift of the storm track (Kawase et al. 2021). There is a difference on the Sea of Japan side of eastern Japan, partly due to the differences in the topography between the model resolutions and in the representation of topographic precipitation between the AGCM and RCM. While the water vapor increases due to the warming contribute to the precipitation increase, weakened northwesterly wind contribute to the precipitation decrease. Such a cancellation makes large uncertainty of the precipitation change over this area. In summer, difference between the simulations is large over western Japan. An increasing trend over northern Japan and a decreasing over the southern coast of eastern Japan are common to the three simulations. It is also common to the simulations using MRI-AGCM (Fig.S3b,d), but is not consistent with the majority of CMIP models, which show slight increase all over Japan (Ose 2019). There is a decrease in the summer mean precipitation and Rx1d only for AGCM20 over the ocean south of Japan (Fig. 3c). As the value of Rx1d in this region is controlled by typhoon activity (Kitoh and Endo 2019), differences in typhoon representation related to model resolution and model physics, as well as uncertainty due to insufficient sample size, could be the cause of the variations seen in the spatial pattens of seasonal and extreme precipitation around Japan.

4. Relationships of changes in extreme precipitation and temperature

Figure 4a shows the time series of the global mean of Rx1d. The percentage increase relative to the 30-year average for the period 1950–1979 is shown. The thin and thick lines show the value for each year and the 10-year running mean, respectively. The pattern of interannual variability is similar among the four simulations. For instance, there are positive peaks in 1998, 2034, and 2070 for all simulations, which correspond to the interannual variability of the prescribed SST. Some decadal variations remain even in the

10-year running mean. For example, there is a large increase from 1980 to 2000, but a small increase from 2000 to 2020. Such variations can be seen even in the latter half of the 21st century, except for RCP8.5, while the large increasing trend in the RCP8.5 simulation dominates the variation. In the RCP8.5 simulations, the increase is slightly smaller in AGCM60 than in AGCM20. This is consistent with the resolution dependence shown in Mizuta and Endo (2020), in which, using the same 60km model, the relative change becomes slightly smaller when Rx1d is calculated after daily precipitation is regridded to 1.25° or 2.5° grid.

Figure 4b–c shows the time series of the 10-year running means of Rx1d averaged over land in Japan. The four AGCM60 (Fig. 4b) and four RCM20 (Fig. 4c) results are compared with the AGCM20 result and the average of the observed data. The observations show no obvious trend until around 1980, but there is an obvious increase after 1995. The increase in Rx1d averaged over 1991–2020 from 1950–1979 is 7.2%. While every single member of AGCM20 and RCM20 simulates the increasing trend in the historical simulation, AGCM60 does not show the increasing trend. Even for the 10-year running means, the time series are noisy, especially for AGCM60 (Fig. 4b), showing large variability on a decadal scale. The difference between the scenarios is not clear even around 2050. The change in the RCP8.5 scenario does not exceed that of all other scenarios until after 2070.

Next, we plotted the relationship between the relative increase in Rx1d and the SAT increase (Fig. 5). For the global average, there is a good correlation between the two values for each year (Fig. 5a), and a much stronger linear correlation for the 10-year running mean (Fig. 5b). The scenario dependence is very small, consistent with the results from CMIP multi-model ensemble mean (Li et al. 2021), with a slope of ~7.5% per degree, which is close to the Clausius–Clapeyron rate of change. It means that the relationship found in the CMIP climate models is valid also for a higher resolution model. Note that, however, this rate of increase varies greatly depending on the timescale of the precipitation and the return period (Mizuta and Endo 2020).

Figure 5c–d shows the same relationship over land in Japan. The results for the 10-year running mean are shown here. AGCM20 and RCM20 (Fig. 5d) show a correlation similar to Fig. 5a. The scenario dependence is small, with a slope of 6% per degree. For AGCM60, on the other hand, the correlation is lower and the slope is smaller, ~4% per degree. It is associated with the smaller increase over northern Japan (Fig. 3f) than those in AGCM20 (Fig. 3c) and RCM20 (Fig. 3i). The smaller slope is partly due to the slight resolution dependence as seen in the global mean (Fig. 4a). The low correlation is mainly due to the result of insufficient grid points over land in Japan in AGCM60 (123 points). Figure S4 shows the relationship over the region of 128–147°E, 30–47°N, which includes 10× larger area than the land in Japan. The relationship in AGCM60 becomes similar to AGCM20 and RCM20, suggesting that it is difficult to evaluate the Rx1d change over land in Japan by a single member of 60km resolution simulation due to too large noise.

5. Summary and concluding remarks

We performed 150-year continuous simulations using AGCM20, and AGCM60 with RCM20 downscaling. The global-mean relative increase in Rx1d was roughly proportional to the increase in the global-mean SAT, especially when viewed as a 10-year running mean, regardless of the emission scenario used. Such a proportional relationship is consistent with previous CMIP multi-model results (Li et al. 2021). Our study shows that the scaling law is valid also for models with a higher resolution than the CMIP climate models. A similar correlation between Rx1d and SAT was seen also in the values averaged over the Japanese land area in AGCM20 and RCM20 after applying a 10-year running mean. Although such a proportional relationship at the regional scale has been suggested by a comparison of +2K and +4K time-slice simulations (Fujita et al. 2019), it becomes clearer by our high-resolution continuous experiment in this study.

These simulations allow us to analyze transitional changes caused by global warming in phenomena that require high-resolution simulations, such as extreme precipitation events. More detailed studies using these simulations are now underway that consider: 1) phenomena that we do not know whether the scaling law with respect to temperature is valid or not (e.g., snow cover, droughts and coastal conservation); 2) areas where the multi-year history of temperature and precipitation is important (e.g., water resources and agriculture); 3) analysis of the timing of the emergence of the change signal from the natural variability; and 4) the scheduling of adaptation policy making.

The proportional relationship between the rate of increase in Rx1d and the SAT increase over the Japanese land area can be seen in AGCM20 and RCM20, but it was not so clear in AGCM60. This is mainly due to the small number of sample grids. When the target spatial and temporal scales become smaller, the effect of internal variability becomes critically larger, which is consistent with previous studies (Hawkins and Sutton 2009). An initial ensemble experiment will be required if we wish to investigate regional-scale extreme precipitation changes at the decadal timescale over the Japan region. In addition, the results presented here are from a single model. Intercomparisons with other HighResMIP simulations, already analyzed for tropical cyclones (Roberts et al. 2020; Yamada et al. 2021), would assist our evaluation of the uncertainty associated with the climate models.

Acknowledgments

The calculations were performed on the Earth Simulator of the Japan Agency for Marine-Earth Science and Technology (JAMSTEC). This work was supported by the Integrated Research Program for Advancing Climate Models (TOUGOU; Grant Number JPMXD0717935561) of the Ministry of Education, Culture, Sports, Science and Technology of Japan, and JSPS KAKENHI grants JP21K03670. The authors thank the two anonymous reviewers whose helpful and constructive comments helped to improve this manuscript.

Data Availability Statement

Data of the RCP8.5 experiments with AGCM20 and AGCM60 are publicly available as the CMIP6 HighResMIP through the Earth System Grid Federation (https://esgf-node.llnl.gov/projects/cmip6/). AGCM60 and RCM20 data will be available from the Data Integration and Analysis System (DIAS) website (https://diasjp.net/).

Supplements

Supplement 1: One table and four supplemental figures are included.

References

Collins, M., et al. (2013), Long-term climate change: Projections, commitments and irreversibility, in Climate Change 2013: The Physical Science Basis. Contribution of Working Group I to the Fifth Assessment Report of the Intergovernmental Panel on Climate Change, edited by T. F. Stocker et al. Cambridge Univ. Press, Cambridge, U. K., and New York.

Eyring, V., S. Bony, G. A. Meehl, C. Senior, B. Stevens, R. J. Stouffer, and K. E. Taylor, 2016: Overview of the Coupled Model Intercomparison Project Phase 6 (CMIP6) experimental design and organization. *Geosci. Model Dev.*, 9, 1937–1958.

Fujita, M., R. Mizuta, M. Ishii, H. Endo, T. Sato, Y. Okada, S. Kawazoe, S. Sugimoto, K. Ishihara, and S. Watanabe, 2019: Precipitation changes in a climate with 2-K surface warming from large ensemble simulations using 60-km global and 20-km regional atmospheric models. *Geophys. Res. Lett.*, 46, 435-442, doi:10.1029/2018GL079885.

Haarsma, R. J., M. Roberts, P. L. Vidale, C. A. Senior, A. Bellucci, Q. Bao, P. Chang, S. Corti, N. S. Fučkar, V. Guemas, J. von Hardenberg, W. Hazeleger, C. Kodama, T. Koenigk, L.-Y. R. Leung, J. Lu, J.-J. Luo, J. Mao, M. S. Mizielinski, R. Mizuta, P. Nobre, M. Satoh, E. Scoccimarro, T. Semmler, J. Small, and J.-S. von Storch, 2016:

High Resolution Model Intercomparison Project (HighResMIP v1.0) for CMIP6. *Geosci. Model Dev.*, 9, 4185–4208, doi:10.5194/gmd-9-4185-2016.

Hawkins, E., and R. Sutton, 2009: The potential to narrow uncertainty in regional climate predictions. *Bull. Amer. Meteor. Soc.*, 90, 1095–1107. doi:10.1175/2009BAMS2607.1

Hawkins, E., Frame, D., Harrington, L., Joshi, M., King, A., Rojas, M., and Sutton, R. (2020). Observed emergence of the climate change signal: From the familiar to the unknown. *Geophys. Res. Lett.*, 47, e2019GL086259. doi:10.1029/2019GL086259

Imada, Y., H. Kawase, M. Watanabe, M. Arai, H. Shiogama, and I. Takayabu, 2020: Advanced risk-based event attribution for heavy regional rainfall events. *npj Clim Atmos Sci*, 3, 37 (2020). doi:10.1038/s41612-020-00141-y

Ishii, M., and N. Mori, 2020: d4PDF: large-ensemble and high-resolution climate simulations for global warming risk assessment. *Prog. Earth Planet. Sci.*, 7, doi:10.1186/s40645-020-00367-7.

Japan Meteorological Agency, 2021: Climate change monitoring report 2020. https://www.jma.go.jp/jma/en/NMHS/ccmr/ccmr2020.pdf.

Kawase, H., A. Murata, K. Yamada, T. Nakaegawa, R. Ito, R. Mizuta, M. Nosaka, S. Watanabe, and H. Sasaki, 2021: Regional characteristics of future changes in snowfall in Japan under RCP2.6 and RCP8.5 scenarios. *SOLA*, 17, 1−7, doi:10.2151/sola.2021-001.

Kennedy, J., H. Titchner, N. Rayner, and M. Roberts, 2017: input4MIPs. MOHC. SSTsAndSeaIce. HighResMIP. MOHC-HadISST-2-2-0-0-0. Earth System Grid Federation. doi:10.22033/ESGF/input4MIPs.1221.

Kitoh, A., and H. Endo, 2016: Changes in precipitation extremes projected by a 20-km mesh global atmospheric model. *Weather and Climate Extremes*, 11, 41−52.

Kitoh, A., T. Ose, and I. Takayabu, 2016: Dynamical downscaling for climate projection with high-resolution MRI AGCM-RCM. *J. Meteor. Soc. Japan*, 94A, 1–16, doi:10.2151/jmsj.2015-022.

Kitoh, A., and H. Endo (2019). Future changes in precipitation extremes associated with tropical cyclones projected by large-ensemble simulations. *J. Meteor. Soc. Japan*, 97, 141–152.

Kusunoki, S., and R. Mizuta, 2013: Changes in precipitation intensity over East Asia during the 20th and 21st centuries simulated by a global atmospheric model with a 60 km grid size. *J. Geophys. Res.*, 118, 11007-11016, doi:10.1002/jgrd.50877.

Li, C., Zwiers, F., Zhang, X., Li, G., Sun, Y., and Wehner, M. (2021). Changes in Annual Extremes of Daily Temperature and Precipitation in CMIP6 Models, *J. Climate*, 34(9), 3441-3460, doi:10.1175/JCLI-D-19-1013.1.

Mizuta, R., H. Yoshimura, H. Murakami, M. Matsueda, H. Endo, T. Ose, K. Kamiguchi, M. Hosaka, M. Sugi, S. Yukimoto, S. Kusunoki, and A. Kitoh, 2012: Climate simulations using MRI-AGCM3.2 with 20-km grid. *J. Meteor. Soc. Japan*, 90A, 233–258.

Mizuta, R., O. Arakawa, T. Ose, S. Kusunoki, H. Endo, and A. Kitoh, 2014: Classification of CMIP5 future climate responses by the tropical sea surface temperature changes. *SOLA*, 10, 167−171.

Mizuta, R., A. Murata, M. Ishii, H. Shiogama, K. Hibino, N. Mori, O. Arakawa, Y. Imada, K. Yoshida, T. Aoyagi, H. Kawase, M. Mori, Y. Okada, T. Shimura, T. Nagatomo, M. Ikeda, H. Endo, M. Nosaka, M. Arai, C. Takahashi, K. Tanaka, T. Takemi, Y. Tachikawa, K. Temur, Y. Kamae, M. Watanabe, H. Sasaki, A. Kitoh, I. Takayabu, E. Nakakita, and M. Kimoto, 2017: Over 5000 years of ensemble future climate simulations by 60 km global and 20 km regional atmospheric models. *Bull. Amer. Meteor. Soc.*, 98, 1383–1398, doi:10.1175/BAMS-D-16-0099.1.

Mizuta, R., and H. Endo, 2020: Projected changes in extreme precipitation in a 60-km AGCM large ensemble and their dependence on return periods, *Geophys. Res. Lett.*, 47, e2019GL086855. doi:10.1029/2019GL086855.

Murata, A., H. Sasaki, H. Kawase, M. Nosaka, M. Oh'izumi, T. Kato, T. Aoyagi, F. Shido,

K. Hibino, S. Kanada, A. SuzukiParker, and T. Nagatomo, 2015: Projection of future climate change over Japan in ensemble simulations with a highresolution regional climate model. *SOLA*, 11, 90–94.

Nosaka, M., M. Ishii, H. Shiogama, R. Mizuta, A. Murata, H. Kawase, and H. Sasaki, 2020: Scalability of future climate changes across Japan examined with large-ensemble simulations at +1.5 K, +2 K, and +4 K global warming levels. *Prog. Earth Planet. Sci.*, 7, doi:10.1186/s40645-020-00341-3.

O'Neill, B. C., Tebaldi, C., van Vuuren, D. P., Eyring, V., Friedlingstein, P., Hurtt, G., Knutti, R., Kriegler, E., Lamarque, J.-F., Lowe, J., Meehl, G. A., Moss, R., Riahi, K., and Sanderson, B. M.: The Scenario Model Intercomparison Project (ScenarioMIP) for CMIP6, *Geosci. Model Dev.*, 9, 3461-3482, doi:10.5194/gmd-9-3461-2016, 2016

Ose, T., 2019: Future changes in summertime East Asian monthly precipitation in CMIP5 and their dependence on present-day model climatology. *J. Meteor. Soc. Japan*, 97, 1041–1053, doi:10.2151/jmsj.2019-055.

Roberts, M. J., J. Camp, J. Seddon, P. L. Vidale, K. Hodges, B. Vannière, J. Mecking, R. Haarsma, A. Bellucci, E. Scoccimarro, L.-P. Caron, F. Chauvin, L. Terray, S. Valcke, M.-P. Moine, D. Putrasahan, C. D. Roberts, R. Senan, C. Zarzycki, P. Ullrich, Y. Yamada, R. Mizuta, C. Kodama, D. Fu, Q. Zhang, G. Danabasoglu, N. Rosenbloom, H. Wang, and L. Wu, 2020: Projected future changes in tropical cyclones using the CMIP6 HighResMIP multimodel ensemble. *Geophys. Res. Lett.*, 47, e2020GL088662. doi:10.1029/2020GL088662.

Sasaki, H., K. Kurihara, I. Takayabu, and T. Uchiyama, 2008: Preliminary experiments of reproducing the present climate using the non-hydrostatic regional climate model, *SOLA*, 4, 25–28.

Sugi, M., and J. Yoshimura, 2012: Decreasing Trend of Tropical Cyclone Frequency in 228-year High-resolution AGCM Simulations. *Geophys. Res. Let.*, 39, L19805.

Yamada, Y., C. Kodama, M. Satoh, M. Sugi, M. J. Roberts, R. Mizuta, A. T. Noda, T.

Nasuno, M. Nakano, and P. L. Vidale, 2021: Evaluation of the contribution of tropical cyclone seeds to changes in tropical cyclone frequency due to global warming in high-resolution multi-model ensemble simulations. *Prog. Earth Planet Sci.*, 8, 11. doi:10.1186/s40645-020-00397-1

Yukimoto, S., H. Kawai, T. Koshiro, N. Oshima, K. Yoshida, S. Urakawa, H. Tsujino, M. Deushi, T. Tanaka, M. Hosaka, S. Yabu, H. Yoshimura, E. Shindo, R. Mizuta, A. Obata, Y. Adachi, and M. Ishii, 2019: The Meteorological Research Institute Earth System Model Version 2.0, MRI-ESM2.0: Description and Basic Evaluation of the Physical Component. *J. Meteor. Soc. Japan*, 97, 931–965, doi:10.2151/jmsj.2019-051.

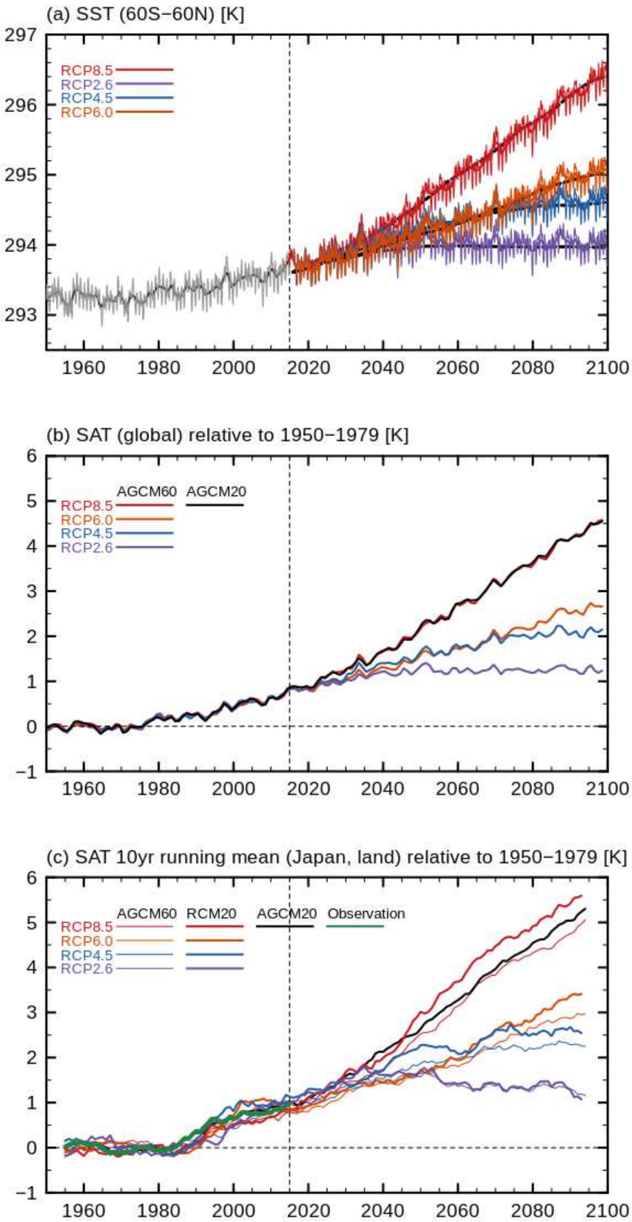

Fig. 1. (a) Time series of SSTs prescribed for the AGCM simulations averaged over 60°S–60°N. Thin lines are monthly-mean values and thick lines are annual-mean values. Thick black dashed lines after 2015 show the warming trends without interannual variability calculated from the CMIP5 model experiments. (b) Time series of the global-mean annual-mean SAT change from the 30-year average of 1950–1979. (c) As (b), but 10-year running-mean values averaged over the Japanese land grids, including the average of observed data.

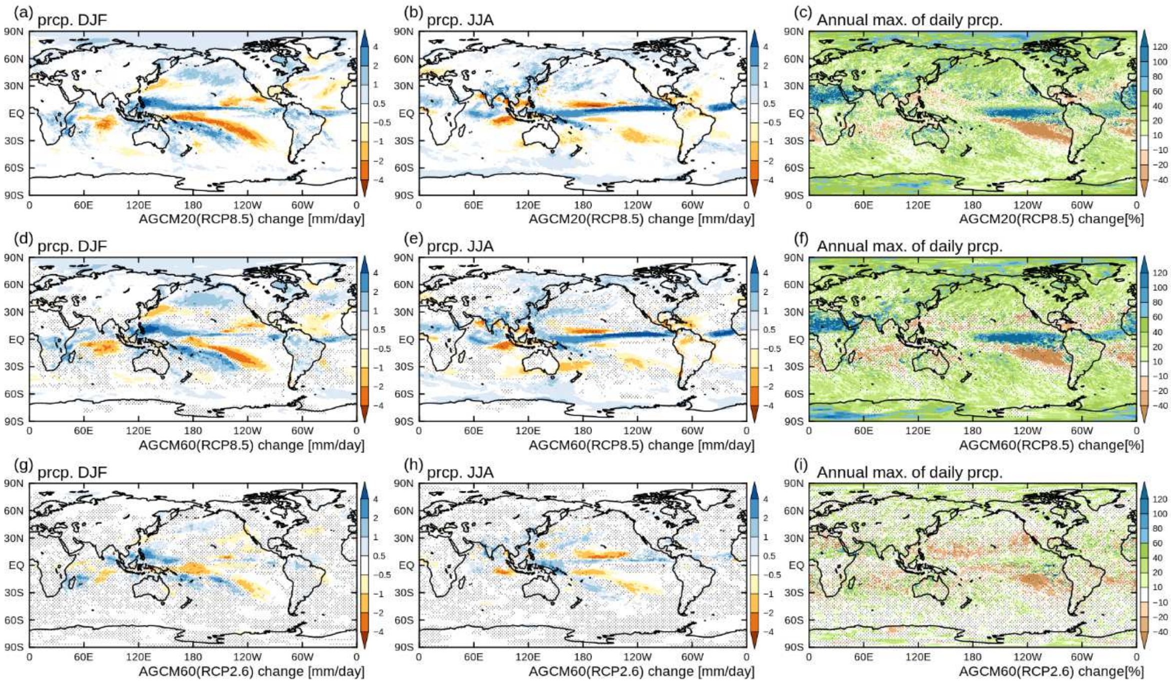

Fig. 2. Horizontal distribution of the changes from 1979–2003 to 2075–2099 for (a, d, g) mean precipitation from December to February (mm/day), (b, e, h) mean precipitation from June to August (mm/day), and (c, f, i) relative changes in Rx1d (%), using (a–c) RCP8.5 with AGCM20, (d–f) RCP8.5 with AGCM60, and (g–i) RCP2.6 with AGCM60. The hatches in (d-i) indicate that the change is not statistically significant at the 95 % level against the ensemble spread, calculated from the four-member historical simulations.

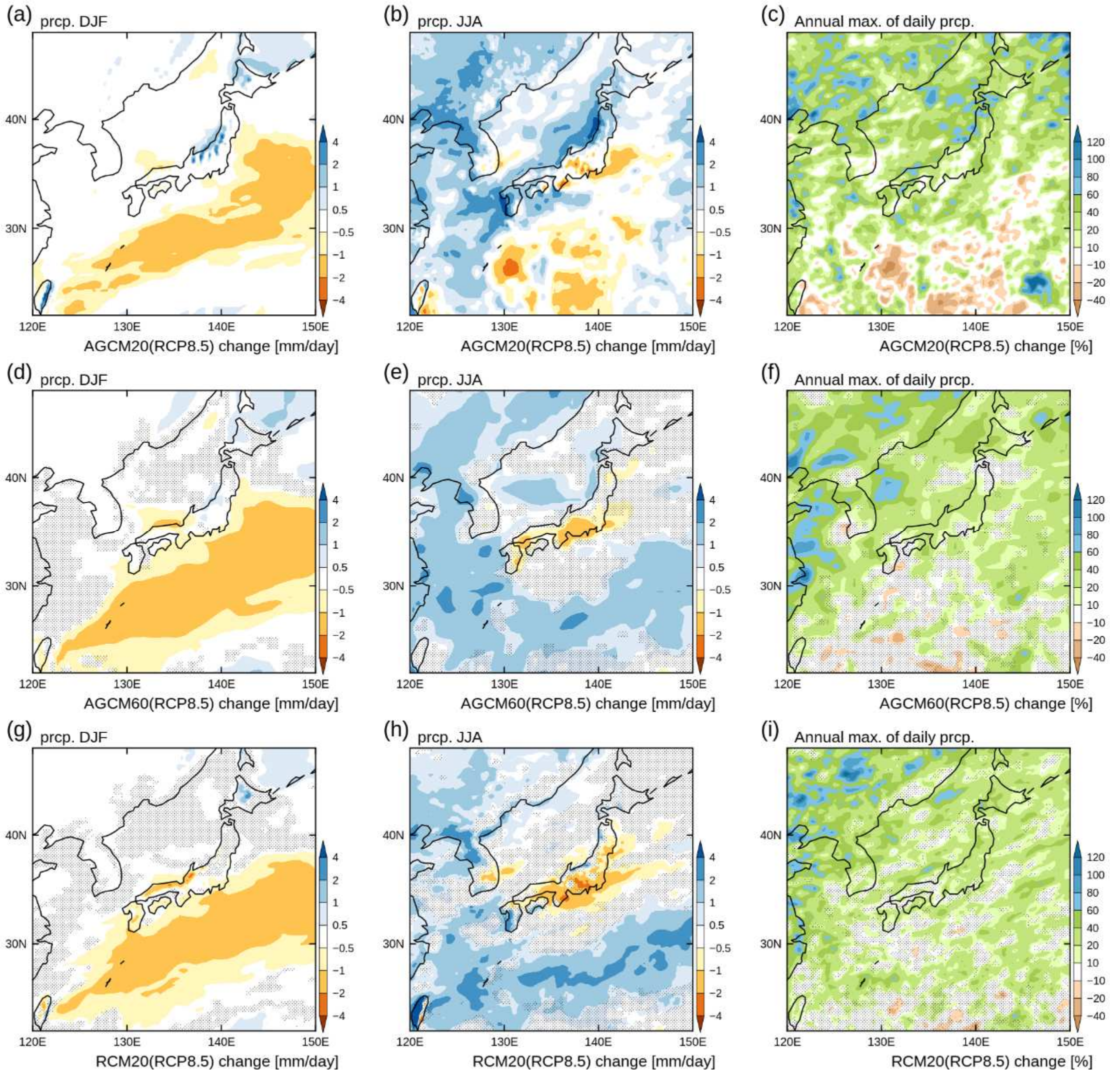

Fig. 3. As Fig. 2, but around Japan, using RCP8.5 with (a–c) AGCM20, (d–f) AGCM60, and (g–i) RCM20.

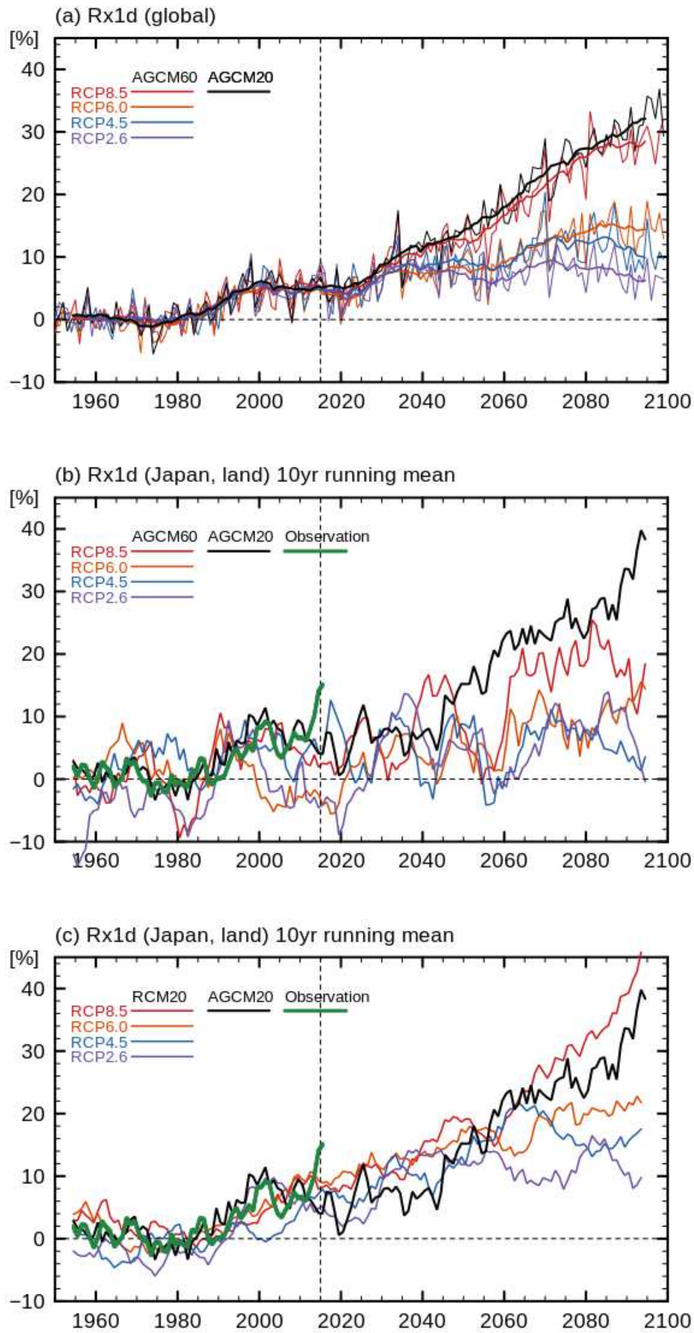

Fig. 4. (a) Time series of the global mean of Rx1d change relative to the 30-year average over the period 1950–1979. Thin lines are the value for each year, and the thick lines are the 10-year running mean. (b, c) As (a), but showing the 10-year running-mean values averaged over the Japanese land grids, from (b) AGCM60 and (c) RCM20, compared with AGCM20 and the average of the observed data.

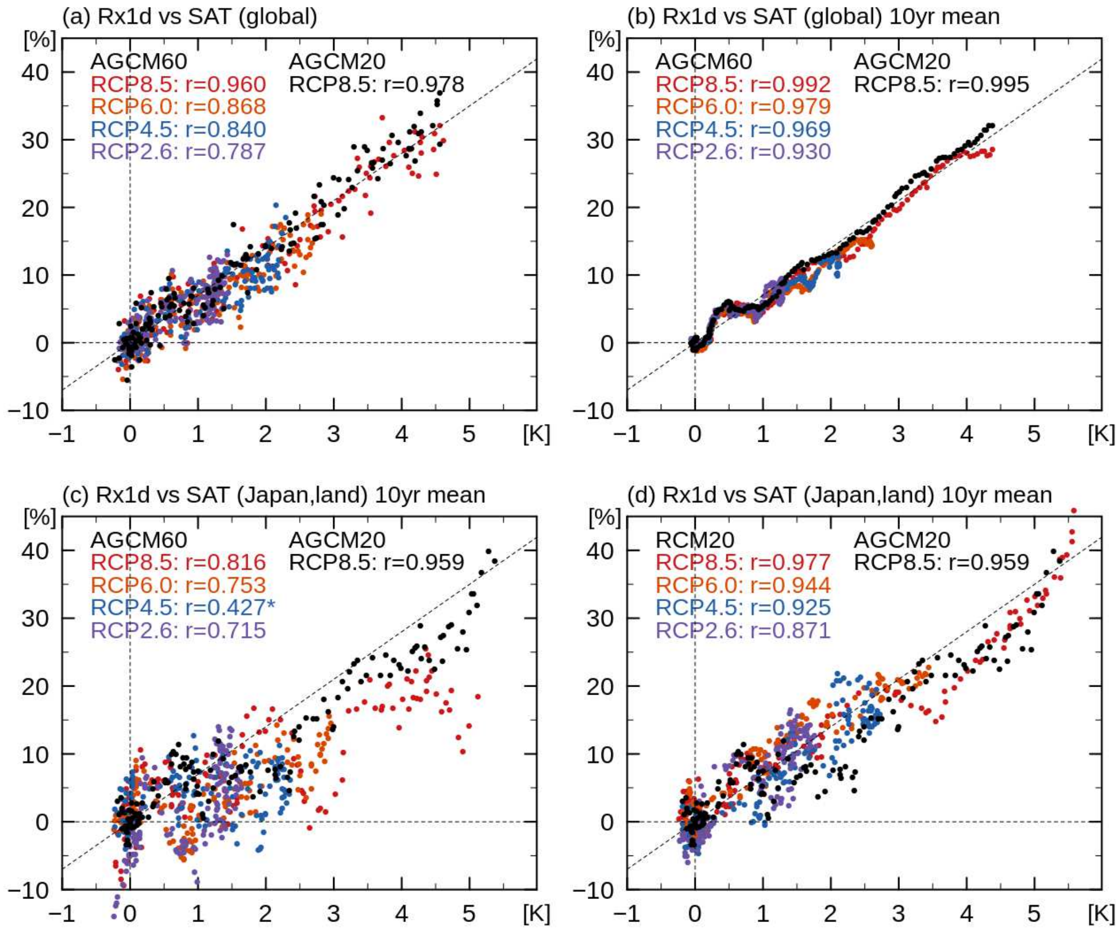

Fig. 5. Scatter plots of relative change in Rx1d (%) and SAT change (K), for (a) global-mean values for each year, (b) global-mean values for 10-year running mean, (c, d) 10-year running mean values averaged over the Japanese land grids, from (b) AGCM60 and (c) RCM20, compared with AGCM20. The changes are relative to the 30-year average over the period 1950–1979. The dashed line indicates a slope of 7% per degree. The correlation coefficients are calculated using 10-year means of every 10 years. Asterisks denote that the correlation is not statistically significant at the 99% significance level.